



Crucial properties of the moment closure model FENE-QE

Han Wang, Kun Li, Pingwen Zhang*

LMAM and School of Mathematical Sciences, Peking University, Beijing 100871, PR China

Received 22 April 2007; received in revised form 16 October 2007; accepted 16 October 2007

Abstract

We investigate four crucial properties for testing and evaluating a moment closure approximation of the FENE dumbbell model for dilute polymer solutions: non-negative configuration distribution function, energy dissipation, accuracy of approximation and computational expense. Through mathematical analysis, numerical experiments and comparisons with closure model FENE-P and FENE-YDL, we prove that the FENE-QE approximation has non-negative configuration distribution function, approximates the energy dissipation behavior of original kinetic theory and provides good accuracy. To improve the efficiency of this closure approximation, we introduce a piecewise linear approximation technique that greatly reduces the computational cost. This extension of FENE-QE, FENE-QE-PLA, is the closure model we recommend for simulating dilute polymer solutions.

© 2007 Elsevier B.V. All rights reserved.

Keywords: Constitutive equation; Kinetic theory; FENE dumbbells; Closure approximation; Quasi-equilibrium approximation

1. Introduction

The dynamics of dilute polymer fluids is an interesting issue because its rheological behavior is significantly different from Newtonian fluids. The continuum fluid mechanics coupled with the kinetic approach can be viewed as a complementary way to describe the flow of dilute polymer solutions. The continuum fluid mechanics concerns the dynamics of macroscopic physical variables such as velocity, pressure and energy of the fluid. Kinetic theory provides microscopic configuration information about polymer solutes which cause the non-Newtonian rheological behavior of dilute polymer fluids. The simplest and most widely used non-linear kinetic model is known as the Warner finite extensible non-linear elastic (FENE) dumbbell model. In this paper, we only consider polymer fluids that can be modeled as FENE dumbbell.

Kinetic theory can be viewed from two points of view. In the first way, kinetic theory is written as the Fokker–Planck (FP) equation, a partial differential equation (PDE) about the configuration distribution function (CDF). Directly solving FP can become very computationally expensive because of the large number of degrees of freedom. Even though some fast solvers

for FP equation have been designed recently [2,17,18], FP is mostly used in simple cases to simulate the rheological behavior and conformation of dilute polymer fluids. Kinetic theory can also be considered from a stochastic view point. CONNFES-SIT, the representative technique for managing kinetic theory was developed by Laso and Öttinger [13]. This method uses Brownian dynamics simulations that provide micro-information of polymer configuration based on Monte Carlo sampling. In 1997, Hulsen et al. [10] developed a Brownian configuration fields (BCF) method that is widely used as an efficient variant of the original CONNFESSIT. Öttinger et al. [19] pointed out that BCF can be regarded as an extremely powerful extension of variance reduction techniques based on parallel process simulation. The main advantage of these stochastic simulation techniques is the computational cost grows mildly when adding degrees of freedom to the system. Since the statistical error is proportional to $\mathcal{O}(1/\sqrt{N})$, where N is the number of independent samples, we need a large number of samples to improve accuracy. Therefore, limited computational capacity can be viewed as the main barrier to achieve high accuracy using stochastic simulation methods.

In addition, researchers have been revising original kinetic theory and searching for simpler and faster approaches to polymer fluid simulation. This set of approximations are usually referred as closure approximations or closure models. The simplest closure model usually referred as FENE-P is obtained from self-consistent, pre-averaging approximation due to Peter-

* Corresponding author. Tel.: +86 10 6275 9851; fax: +86 10 6276 7146.

E-mail addresses: han_wang@math.pku.edu.cn (H. Wang),
kili@math.pku.edu.cn (K. Li), pzhang@pku.edu.cn (P. Zhang).

lin [1]. Generally speaking, how the closure approximations influence the behavior of the kinetic model is an issue hard to predict theoretically, so that careful numerical experiments are necessary to study the properties of closure approximations. Keunings [12] pointed out that FENE-P gives unphysical results under certain flow conditions. Later, Keunings and his coworkers [15,16] developed FENE-L and FENE-LS approximations that give accurate simulations while avoiding such unphysical phenomena. Various kinds of closure methods have been developed in the last 20 years, for example, FENE-CR (1988) [3], FENE-CD (1999) [21], FENE-DT (2000) [26], FENE-QE (2002) [11] and a closure approximation developed by Yu et al. [28,5]. For convenience and simplicity, we will denote this last model by FENE-YDL. FENE-P and FENE-CR are the most widely used models. They are applied in various practical problems [7,14,23,25] and are compared with experimental data [22]. One can find numerical comparisons of different closure models in [8,15,16,24,26]. Some of these papers develop new closure models and demonstrate the improvements achieved. In the literature, comparisons mainly focus on accuracy. New closure models are developed primarily to achieve better accuracy.

In the present paper, we demonstrate that four properties can be used to evaluate existing closure models and, moreover, are crucial to designing high quality closure models. They are

- non-negative CDF;
- energy dissipation;
- accuracy of approximation;
- computational expense.

It is clear that non-negative is a natural requirement to a probability distribution function. In kinetic theory, we can prove the energy dissipation property, so the closure model that preserves this property will be more reliable in this respect. The accuracy of approximation can be divided into two aspects. Microscopically, we will investigate the approximation quality of CDF that describes the direction and extension of dumbbell-shaped molecules in the flow. Macroscopically, we will investigate the accuracy of the stress tensor calculated by closure models. Sometimes, the two aspects can produce inconsistent results, that is some closure models that give poor approximation to microscopic CDF can calculate stress tensor accurately. A closure approximation of high quality is supposed to reduce deviation in both aspects. The original FENE model is the most accurate, but the computational cost is unacceptable in most cases. Most closure models can reduce the computational cost in a dramatic way. This is achieved by concentrating on macroscopic variables (moments in most cases) that can reflect the configuration of FENE dumbbells rather than calculating configuration distribution directly. Even if applying closure approximations can save a lot of time, some closure models can also be very computationally expensive, for example FENE-QE. A high quality closure model should be computationally cheap.

In this paper, we pay close attention to closure model FENE-QE [11] where QE stands for quasi-equilibrium approximation. Numerical experiments for FENE-P and FENE-YDL are used for comparison. The four properties mentioned above are inves-

tigated in both analytical and numerical ways. We find that FENE-QE is a model of non-negative CDF, correct energy dissipation and high accuracy. To reduce the computational cost of FENE-QE, we design a piecewise linear approximation (PLA) technique that can improve the efficiency of FENE-QE greatly and have little effect on its accuracy.

This paper is arranged as follows, In Section 2, we will introduce kinetic theory for dilute polymer solutions and prove the energy dissipation of it. In Section 3, we will introduce the FENE-QE model and the PLA technique and prove the correctness of its energy dissipation. In Section 4, FENE-QE as well as FENE-P and FENE-YDL are used to calculate steady shear flow and elongational flow. In Section 5, the lid-driven cavity serves as a example of a coupled system with a complex fluid field. In Section 6, we conclude that FENE-QE with PLA technique satisfies the four crucial properties and can be viewed as a high quality closure model.

2. Kinetic model of dilute polymer solutions

The flexible solute polymer can be abstracted as a series of beads connected by springs. In this paper we only consider the dumbbell model; a simplified case in which two beads are connected by one spring. If the position of the two beads are \mathbf{r}_1 and \mathbf{r}_2 , respectively, then the connector vector of them is defined by $\mathbf{Q} = \mathbf{r}_1 - \mathbf{r}_2$. \mathbf{Q} reflects the configuration of the dumbbell-shaped polymer. The CDF as a function of connector vector and time is denoted by $f(\mathbf{Q}, t)$. Let S be the entropy of the isolated isothermal solution system. We assume $kT = 1$, so it will not be taken into account through our paper:

$$S[f] = n \left(- \int f \ln f - f d\mathbf{Q} \right) \quad (1)$$

From it, we define the free energy by

$$A[f] = -S[f] + n \int Uf d\mathbf{Q} \quad (2)$$

where n is the polymer number density and U is the elastic spring potential. The widely used FENE dumbbell spring potential is

$$U = -\frac{HQ_0^2}{2} \log \left[1 - \left(\frac{\mathbf{Q}}{Q_0} \right)^2 \right] \quad (3)$$

The equilibrium state is formed when the free energy reaches its minimum value. One necessary condition is

$$\left. \frac{\delta A}{\delta f} \right|_{f=f_{\text{eq}}} = 0 \quad (4)$$

Starting from (4), one can easily reach

$$f_{\text{eq}} \propto e^{-U} = \left[1 - \left(\frac{\mathbf{Q}}{Q_0} \right)^2 \right]^{HQ_0^2/2} \quad (5)$$

For convenience, we introduce the chemical potential μ defined by

$$\mu = \frac{\delta A}{\delta f} = n(\ln f + U) \quad (6)$$

The dynamics of CDF is given by the famous FP equation:

$$\frac{\partial f}{\partial t} = \nabla_{\mathbf{Q}} \cdot \left(\frac{2}{n\zeta} f \nabla_{\mathbf{Q}} \mu \right) \quad (7)$$

$$\frac{\partial f}{\partial t} = \frac{2}{\zeta} \nabla_{\mathbf{Q}} \cdot (\mathbf{F}^c f) + \frac{2}{\zeta} \Delta_{\mathbf{Q}} f \quad (8)$$

where \mathbf{F}^c is the connector force which can be expressed as the gradient of the elastic spring potential $\mathbf{F}^c = \nabla_{\mathbf{Q}} U$. Now we consider the dynamics of free energy (the methodology we used here is actually the same as that developed by Yu et al. [27]):

$$\begin{aligned} \frac{dA}{dt} &= \left(\frac{\delta A}{\delta f}, \frac{\partial f}{\partial t} \right) = \left(\mu, \nabla_{\mathbf{Q}} \cdot \left(\frac{2}{n\zeta} f \nabla_{\mathbf{Q}} \mu \right) \right) \\ &= - \left(\nabla_{\mathbf{Q}} \mu, \frac{2}{n\zeta} f \nabla_{\mathbf{Q}} \mu \right) \end{aligned} \quad (9)$$

That the derivative of free energy over time is negative definite implies the energy dissipation properties of kinetic theory.

A general dumbbell model for dilute polymer solutions in the background of macroscopic flow field can be described by a coupled system of divergence free (incompressible) Navier–Stokes equations:

$$\frac{\partial \mathbf{u}}{\partial t} + \mathbf{u} \cdot \nabla \mathbf{u} + \nabla p = \nabla \cdot \boldsymbol{\tau}_p + \nu \Delta \mathbf{u} \quad (10)$$

$$\nabla \cdot \mathbf{u} = 0 \quad (11)$$

and a FP equation of CDF

$$\frac{\partial f}{\partial t} + \mathbf{u} \cdot \nabla_x f + \nabla_{\mathbf{Q}} \cdot (\boldsymbol{\kappa} \cdot \mathbf{Q} f) = \frac{2}{\zeta} \nabla_{\mathbf{Q}} \cdot (\mathbf{F}^c f) + \frac{2}{\zeta} \Delta_{\mathbf{Q}} f \quad (12)$$

Here we denote \mathbf{x} as spacial point. In Eqs. (10)–(12), $\mathbf{u} = \mathbf{u}(\mathbf{x}, t)$ and $f = f(\mathbf{x}, \mathbf{Q}, t)$ are the macroscopic velocity field and CDF, respectively. The variable p is the hydrostatic pressure, ν is the solvent fluid viscosity, $\boldsymbol{\kappa} = (\nabla_x \mathbf{u})^T$ is the velocity gradient and $\boldsymbol{\tau}_p$ is a polymer stress whose relationship with the configuration distribution is described by Kramers' expression:

$$\boldsymbol{\tau}_p = \langle \mathbf{Q} \nabla_{\mathbf{Q}} \mu \rangle = -n\mathbf{I} + n \langle \mathbf{Q} \mathbf{F}^c \rangle \quad (13)$$

Here $\langle \cdot \rangle$ is an average over CDF. Similarly, one can prove the energy dissipation of the coupled system by defining

$$A[f] = n \left(\int \frac{1}{2} \mathbf{u} \cdot \mathbf{u} \, d\mathbf{x} + \iint f \ln f - f + fU \, d\mathbf{Q} \, d\mathbf{x} \right) \quad (14)$$

3. Quasi-equilibrium approximation and PLA technique

3.1. Quasi-equilibrium approximation

The quasi-equilibrium approximation is based on the minimum energy principle under certain constraints:

$$\min A[f] \quad (15)$$

$$\text{s.t.} \quad \int \mathbf{m}(\mathbf{Q}) f \, d\mathbf{Q} = \mathbf{M} \quad (16)$$

Here \mathbf{M} are values of some macroscopic variables and \mathbf{m} are corresponding functions of connector vector \mathbf{Q} . The solution to (15) and (16) is called the quasi-equilibrium (QE) state. The solution to the constrained optimization problem is given by

$$\begin{aligned} \frac{\delta}{\delta f} \left\{ \int f \ln f - f + fU \, d\mathbf{Q} - \boldsymbol{\Lambda} \cdot \left[\int \mathbf{m}(\mathbf{Q}) f \, d\mathbf{Q} - \mathbf{M} \right] \right\} = 0 \end{aligned} \quad (17)$$

where $\boldsymbol{\Lambda}$ are Lagrangian multipliers. The solution of (17) is

$$f_{\mathbf{M}} = \exp\{-U + \boldsymbol{\Lambda} \cdot \mathbf{m}\} \quad (18)$$

According the definition of \mathbf{M} (16) and the dynamics of f (7), we can deduce the dynamics of the macroscopic variables:

$$\frac{\partial \mathbf{M}}{\partial t} = \left(\mathbf{m}, \frac{\partial f}{\partial t} \right) \Big|_{f=f_{\mathbf{M}}} = \int \mathbf{m} \nabla_{\mathbf{Q}} \cdot \left(\frac{2}{n\zeta} f_{\mathbf{M}} \nabla_{\mathbf{Q}} \mu \right) \, d\mathbf{Q} \quad (19)$$

We can prove that the energy dissipation behavior of QE state mimics kinetic theory by the following argument. (We also share the same methodology developed by [27].)

$$\frac{dA(\mathbf{M})}{dt} = \frac{\partial A}{\partial \mathbf{M}} \cdot \frac{\partial \mathbf{M}}{\partial t} = \frac{\partial A}{\partial \mathbf{M}} \cdot \left(\mathbf{m}, \frac{\partial f}{\partial t} \right) \Big|_{f=f_{\mathbf{M}}} \quad (20)$$

Here, $A(\mathbf{M}) = A[f_{\mathbf{M}}]$ is the free energy of the closure model. As a lemma, we can prove the following relation:

$$\begin{aligned} \frac{\partial A}{\partial \mathbf{M}} &= \lim_{t \rightarrow 0} \frac{A(\mathbf{M} + t\Delta\mathbf{M}) - A(\mathbf{M})}{t\Delta\mathbf{M}} \\ &= \lim_{t \rightarrow 0} \frac{A[f_{\mathbf{M} + t\Delta f}] - A[f_{\mathbf{M}}]}{t(\mathbf{m}, \Delta f)} \\ &= \frac{(\delta A / \delta f, t\delta f) \Big|_{f=f_{\mathbf{M}}}}{t(\mathbf{m}, \Delta f)} = n\boldsymbol{\Lambda} \end{aligned} \quad (21)$$

Therefore

$$\frac{dA(\mathbf{M})}{dt} = \left(\frac{\delta A}{\delta f}, \frac{\partial f}{\partial t} \right) \Big|_{f=f_{\mathbf{M}}} = \frac{dA[f]}{dt} \Big|_{f=f_{\mathbf{M}}} \leq 0 \quad (22)$$

This relation not only tells us that the QE model preserves the energy dissipation property, but also shows that the energy dissipation approximates the original dissipation process.

Actually the quasi-equilibrium approximation itself and the result of energy dissipation are more general. They can be

applied not only to FENE dumbbell but also to other kinetic models.

Usually, the macroscopic variables \mathbf{M} are chosen as moments of the connector vector. In this paper, we will only employ the second moment given by $\mathbf{M} = \langle \mathbf{Q} \mathbf{Q} \rangle$ and the corresponding $\mathbf{m}(\mathbf{Q}) = \mathbf{Q} \mathbf{Q}$. In addition, we will apply the constraint $\int f d\mathbf{Q} = 1$, which is equal to a constraint on the zeroth moment. From general QE theory, we can reach

$$f(\mathbf{Q}) = \frac{1}{Z(\mathbf{R})} \left[1 - \left(\frac{\mathbf{Q}}{Q_0} \right)^2 \right]^{HQ_0^2/2} \exp \{ \mathbf{R} : \mathbf{Q} \mathbf{Q} \} \quad (23)$$

where $Z(\mathbf{R})$ is defined by

$$Z(\mathbf{R}) = \int \left[1 - \left(\frac{\mathbf{Q}}{Q_0} \right)^2 \right]^{HQ_0^2/2} \exp \{ \mathbf{R} : \mathbf{Q} \mathbf{Q} \} d\mathbf{Q} \quad (24)$$

\mathbf{R} is the Lagrangian multiplier in matrix form and can be determined from the constraint.

$$\mathbf{M} = \frac{1}{Z(\mathbf{R})} \int \mathbf{Q} \mathbf{Q} \left[1 - \left(\frac{\mathbf{Q}}{Q_0} \right)^2 \right]^{HQ_0^2/2} \exp \{ \mathbf{R} : \mathbf{Q} \mathbf{Q} \} d\mathbf{Q} \quad (25)$$

Further, we can write the dynamics of the second moment as

$$\frac{\partial \mathbf{M}}{\partial t} + \mathbf{u} \cdot \nabla \mathbf{M} - \kappa \cdot \mathbf{M} - \mathbf{M} \cdot \kappa^T = -\frac{4}{\zeta} (\mathbf{R} \cdot \mathbf{M} + \mathbf{M} \cdot \mathbf{R}) \quad (26)$$

Finally, the polymer stress tensor can be expressed as

$$\boldsymbol{\tau}_p = n(\mathbf{R} \cdot \mathbf{M} + \mathbf{M} \cdot \mathbf{R}) \quad (27)$$

3.2. PLA technique

When solving Eq. (26), one has to calculate the Lagrangian multiplier \mathbf{R} from moment \mathbf{M} at each time level. This is a difficult job because the mapping from \mathbf{M} to \mathbf{R} is given implicitly by (25). For convenience, we denote the right hand side of (25) by $\mathbf{G}(\mathbf{R})$. The mapping $\mathbf{G}(\mathbf{R})$ only depends on the parameter $HQ_0^2/2$ and has no relationship with neither temporal variable t nor spacial variable \mathbf{x} . Calculating \mathbf{R} from a given \mathbf{M} is equal to solving a system of non-linear equations $\mathbf{G}(\mathbf{R}) = \mathbf{M}$. Generally speaking, it is impossible to work out the analytical expression of $\mathbf{R} = \mathbf{G}^{-1}(\mathbf{M})$, so we have to turn to numerical methods for help. Fortunately, according to the symmetry of the domain of $\mathbf{G}(D = \{ \mathbf{Q} : \mathbf{Q} \cdot \mathbf{Q} \leq Q_0^2 \})$, we can prove that \mathbf{M} and \mathbf{R} can be diagonalized by the same orthogonal matrix. Therefore, we can only consider the case when both \mathbf{R} and \mathbf{M} are both diagonal matrices. Further, we can view them as two-dimensional vectors.

A group of direct methods to calculate \mathbf{G}^{-1} are numerical methods solving non-linear systems and one of the most popular methods is Newtonian iteration. Another method that avoids evaluating \mathbf{G}^{-1} is proposed by Öttinger et al. [11] and is based on the dynamics of Lagrangian multiplier \mathbf{R} , which can be easily obtained from a Legendre transform. However, both of the two methods are computationally expensive, especially for coupled systems, because they have to calculate $\mathbf{G}(\mathbf{R})$ and $\nabla \mathbf{G}(\mathbf{R})$ at each

time level. Here we want to point out the fact that the calculation of $\mathbf{G}(\mathbf{R})$ and $\nabla \mathbf{G}(\mathbf{R})$ is a difficult and time consuming part of the computational. Because they are actually integrations of d_c (the dimensional of configuration space) dimensional variables and if the index $HQ_0^2/2$ is small or \mathbf{R} is big, the function to be integrated will become ill-posed with some very sharp peaks introducing numerical difficulties.

Approximate functions to \mathbf{G}^{-1} serve as a group of alternative numerical ways to calculate \mathbf{G}^{-1} . Since \mathbf{G}^{-1} is independent of temporal and spacial variable, the same approximate function can be used for evaluating \mathbf{G}^{-1} at any time and physical position. The expression of the approximate function should be given explicitly and easy to evaluate, so that we can calculate the value of the approximation function at little computational cost.

Till now the problem left is how to approximate \mathbf{G}^{-1} , the snapshot of which is shown in Fig. 1. Obviously, one cannot precisely approximate \mathbf{G}^{-1} by a polynomial. The shape is something like a logarithm function. So maybe one can construct a good approximation based on logarithm functions, but we have not tested this idea. Our method is the piecewise linear approximation (PLA). To explain it clearly, we only need to describe the main processes in the two-dimensional case:

- (1) *Generate a grid on the range of \mathbf{G} .* Since the matrix $\mathbf{M} = \mathbf{G}(\mathbf{R})$ is diagonal, the range of \mathbf{G} can be viewed as a subset of the two-dimensional plane. Further, since matrix \mathbf{M} is positive definite, the range is a subset of the first quadrant. Usually, the grid is generated on a bounded subset of the first quadrant, for example, a uniform grid on $[0.001, 0.5] \times [0.001, 0.5]$. In practice, the grid can be non-uniform.
- (2) *Calculate the value of \mathbf{G}^{-1} at each grid point by Newtonian iteration.* To accelerate the iteration, the initial estimate can be chosen as the value of \mathbf{G}^{-1} on a neighboring grid point.
- (3) *Given any value of \mathbf{M} , calculate $\mathbf{G}^{-1}(\mathbf{M})$ by linear approximation.* We first have to determine in which grid cell the \mathbf{M} is, and then with the known value of \mathbf{G}^{-1} on neighboring grid vertices, we can obtain the value of $\mathbf{G}^{-1}(\mathbf{M})$ by the linear interpolation.

Although it takes time to calculate the value of \mathbf{G}^{-1} for each grid point, these values only depend on the parameter $HQ_0^2/2$. Therefore, once the values of \mathbf{G}^{-1} on grid points are calculated, they can be stored for different problems with the same $HQ_0^2/2$. Numerical experiments shown in Sections 4 and 5 will illustrate that applying the PLA technique improves the efficiency greatly while retaining accuracy.

At last, we want to make some remarks on the grid generation that is the first step of the PLA technique. First of all, we would like to emphasize that the rectangular grid (not necessarily uniform) is usually better than non-rectangular ones. That is because we have to determine in which grid cell a certain \mathbf{M} is at the third step of the PLA and the computational cost of such searching on a non-rectangular grid is $\mathcal{O}(N)$ in general, where N is the total number of grid cells. Even though this cost can be reduced to $\mathcal{O}(\log N)$, it requires more complex techniques and data structures. Whereas the cost of searching on a rectangular

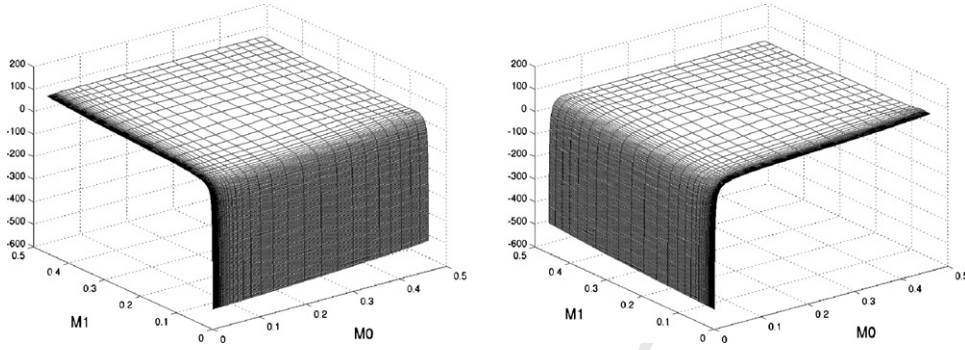


Fig. 1. Snapshot of \mathbf{G}^{-1} , the first component (left) and the second component (right).

grid can be easily reduced to $\mathcal{O}(\log N)$ with the application of the bisection method.

We can generate the grid in a straightforward way: first, form a grid on the domain of \mathbf{G} , and then map it onto the range of \mathbf{G} . The advantage of this way is we can calculate \mathbf{G} instead of \mathbf{G}^{-1} to reform the inverse mapping of \mathbf{G} at the second step of the PLA. The disadvantage is that in two- or three-dimensional cases, we cannot expect the resulting grid is rectangular, when the grid on the domain of \mathbf{G} is generally chosen, for example, a uniform rectangular grid. So we generate the grid in an alternative way. We first generate a grid for the one-dimensional case (with the same parameter $HQ_0^2/2$ as the two-dimensional case) in the straightforward way. Then tensor product the one-dimensional grid and a two-dimensional grid is obtained as a result.

3.3. Other closure approximations

In this paper, we will compare FENE-QE to two additional closure models that also use only second moment, FENE-P [1] and FENE-YDL [28] ($N = 1$ model in [5]). This subsection provides a concise introduction of these additional models.

The FENE-P model is a self-consistent pre-averaging approximation of connector force due to Peterlin. In this model, the connector force is approximated as

$$\mathbf{F}^c \approx \frac{H\mathbf{Q}}{1 - \langle \mathbf{Q}^2 \rangle / Q_0^2} \quad (28)$$

It is easy to derive from the FP equations (12) and (28) an equation for second moment $\mathbf{M} = \langle \mathbf{Q}\mathbf{Q} \rangle$:

$$\begin{aligned} \frac{\partial \mathbf{M}}{\partial t} + \mathbf{u} \cdot \nabla \mathbf{M} - \boldsymbol{\kappa} \cdot \mathbf{M} - \mathbf{M} \cdot \boldsymbol{\kappa}^T \\ = \frac{4}{\zeta} \mathbf{I} - \frac{4H}{\zeta(1 - \text{Tr}(\mathbf{M})/Q_0^2)} \mathbf{M} \end{aligned} \quad (29)$$

In fact, under the Gaussian initial condition, the solution of FP with the Peterlin approximation remains Gaussian [20] and can be written as

$$f(\mathbf{Q}) = \frac{1}{J_G} \exp \left\{ -\frac{1}{2} \mathbf{Q} \cdot \mathbf{M}^{-1} \cdot \mathbf{Q} \right\} \quad (30)$$

where J_G is the scalar such that $\int f d\mathbf{Q} = 1$.

Clearly, the CDF is positive definite. Up to now we cannot prove the energy dissipation of this model. However, Hu and Lelièvre [9] have proved the energy dissipation of the FENE-P model by defining a different kind of entropy. FENE-P model is very simple and the computational cost is small compared to other closure models.

The FENE-YDL model introduces a class of CDFs with the form:

$$f(\mathbf{Q}) = \frac{1}{J_b} \left[1 - \left(\frac{\mathbf{Q}}{Q_0} \right)^2 \right]^{b/2} (1 + \beta Q_1 Q_2 + \gamma(Q_1^2 - Q_2^2)) \quad (31)$$

where J_b is the scalar such that $\int f d\mathbf{Q} = 1$. When b , β and γ take the value HQ_0^2 , 0, and 0, respectively, the configuration distribution reduces to the equilibrium state. One can obtain the evolution of $\langle \mathbf{Q}^2 \rangle$, $\langle Q_1^2 - Q_2^2 \rangle$ and $\langle Q_1 Q_2 \rangle$ from FP equations (12) and (31). We refer readers to [28] for more details.

In fact, under certain conditions, numerical experiments show that the CDF of FENE-YDL can be negative in some regions. The energy dissipation property of kinetic theory is not preserved by this model, even though the leading terms of free energy are the same as those of kinetic theory [28]. It is further shown by [28] that when the state is close to equilibrium, this model is a good approximation of the kinetic model from the view point of energy dissipation. Since only the second moment is concerned, the computational cost of this model is very small and programs of high efficiency can be developed easily.

4. Example: steady shear flow and elongational flow

In this section, the numerical results of three different closure models, FENE-P [1], FENE-YDL [28] and FENE-QE [11], are compared with those of solving FP directly. The effectiveness of the PLA technique is also demonstrated. In both of the two examples, the background flow fields are static and known, so that the dimension of physical space vanishes or is decoupled from FP. Further, we only consider the two-dimensional configuration space for simplicity. Under these assumptions, it is feasible to solve FP directly and the computation of closure models is simplified.

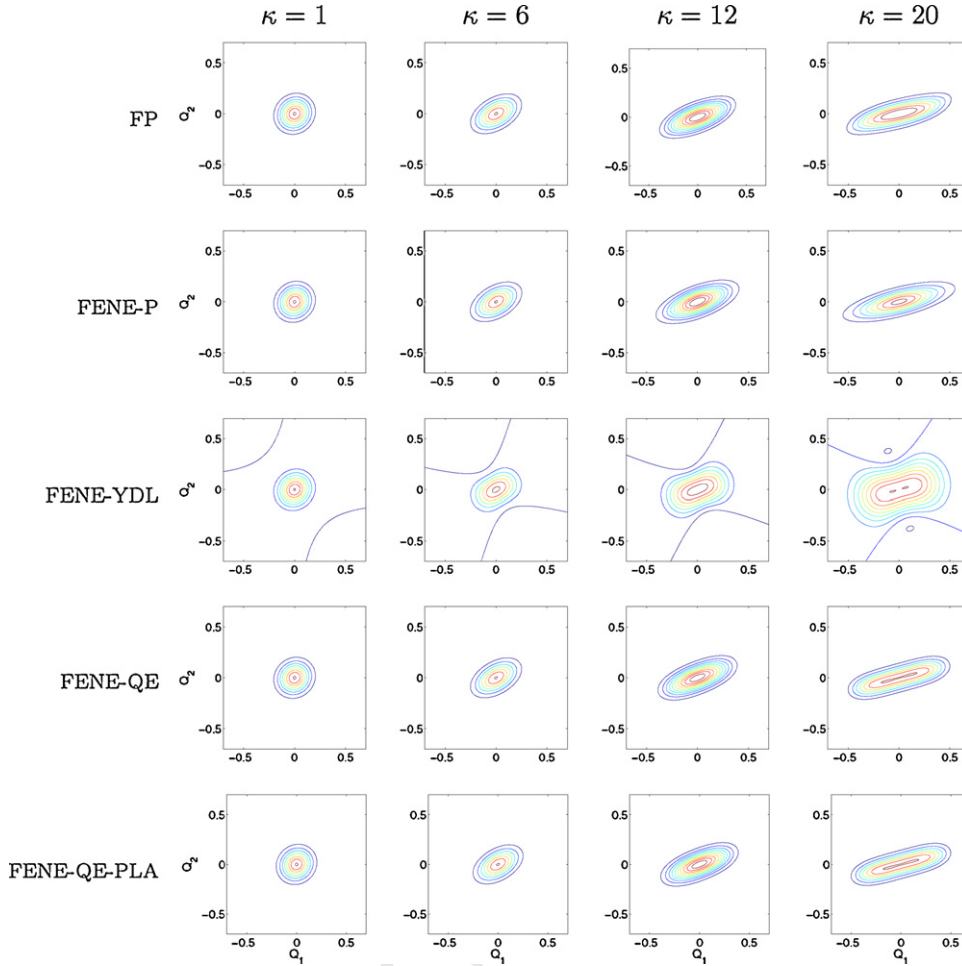


Fig. 2. Shear flow: comparison of the contour plots of CDFs solved from the FP and different closure models for $\kappa = 1, 6, 12$ and 20 .

4.1. Steady shear flow

The static flow field is $\mathbf{u} = (\kappa y, 0)$ where κ is the constant shear rate. In this case the FP reduces to a PDE in the configuration space $\{\mathbf{Q} \in \mathbb{R}^2 : |\mathbf{Q}| < Q_0\}$:

$$\frac{\partial f(\mathbf{Q}, t)}{\partial t} + \frac{\partial}{\partial Q_1}(\kappa Q_2 f) = \frac{2}{\zeta} \nabla_{\mathbf{Q}} \cdot (\mathbf{F}^c f) + \frac{2}{\zeta} \Delta_{\mathbf{Q}} f \quad (32)$$

The configuration space is discretized on an $N \times N$ regular grid covering the square domain $\{\mathbf{Q} : |Q_1| < Q_0, |Q_2| < Q_0\}$ with mesh size $h = 2Q_0/N$. In the computation, we discretize $\partial/\partial Q_2(\kappa Q_2 f)$ and $\nabla_{\mathbf{Q}} \cdot (\mathbf{F}^c f)$ by central difference scheme. We update the value on all points in the circle $|\mathbf{Q}| < Q_0$ whose neighboring points also lie in that circle. This method is equivalent to that described in [5].

In our computations, we use the fourth order explicit Runge–Kutta scheme for time stepping. Physical parameters are chosen as $\zeta = 40$, $H = 100$ and $Q_0 = 1$. The FENE-QE-PLA uses a 203×203 non-uniform rectangular grid. It takes about four hours on a 3 GHz Intel Pentium IV CPU to calculate all values of \mathbf{G}^{-1} on the grid points. The same grid and values are stored for all experiments in this paper. For each choice of κ , Fig. 2 displays CDFs from all models and Table 1 shows the L^1 errors of CDFs. The polymeric normal

stress difference $\tau_p^{11} - \tau_p^{22}$ and shear stress τ_p^{12} are presented in Figs. 3 and 4.

From Fig. 2, we can see that the CDFs of the FENE-P, FENE-QE and FENE-QE-PLA are similar to the results of FP. All of them are non-negative. The results of FENE-YDL are similar to the FP when κ is small, but the deviation becomes very big as κ increases. Moreover, the CDFs of FENE-YDL are not non-negative. Outside the unclosed curves, the CDFs have negative values. From Table 1, we can draw the conclusion that the CDF errors of FENE-QE and FENE-QE-PLA are smaller than those of other closure models. When κ is small, the results of FENE-P are worse than the other closure models. But as κ increases, its

Table 1
Shear flow: L^1 error of the CDFs

κ	FENE-P	FENE-YDL	FENE-QE	FENE-QE-PLA
1	1.10×10^{-2}	4.02×10^{-3}	4.07×10^{-4}	4.17×10^{-4}
3	1.37×10^{-2}	3.68×10^{-2}	9.45×10^{-4}	9.07×10^{-4}
6	2.21×10^{-2}	1.38×10^{-1}	4.43×10^{-3}	4.24×10^{-3}
9	3.49×10^{-2}	2.72×10^{-1}	1.34×10^{-2}	1.29×10^{-2}
12	5.13×10^{-2}	4.13×10^{-1}	3.03×10^{-2}	2.95×10^{-2}
15	6.99×10^{-2}	5.45×10^{-1}	5.73×10^{-2}	5.65×10^{-2}
20	9.97×10^{-2}	7.40×10^{-1}	1.20×10^{-1}	1.19×10^{-1}

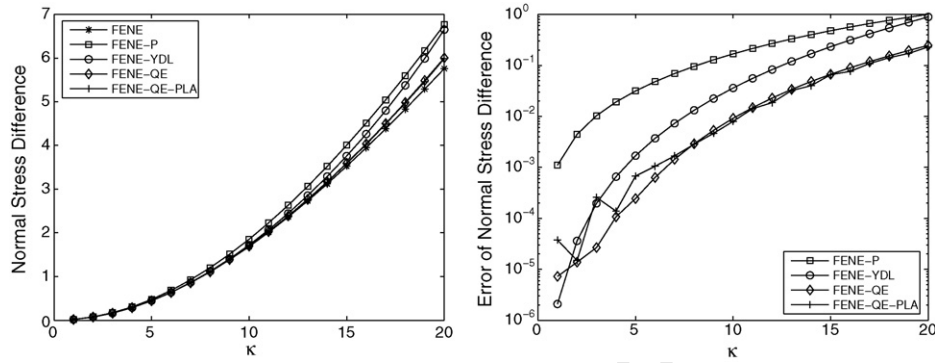


Fig. 3. Shear flow: normal stress difference (left) and the error plot (right) of different methods.

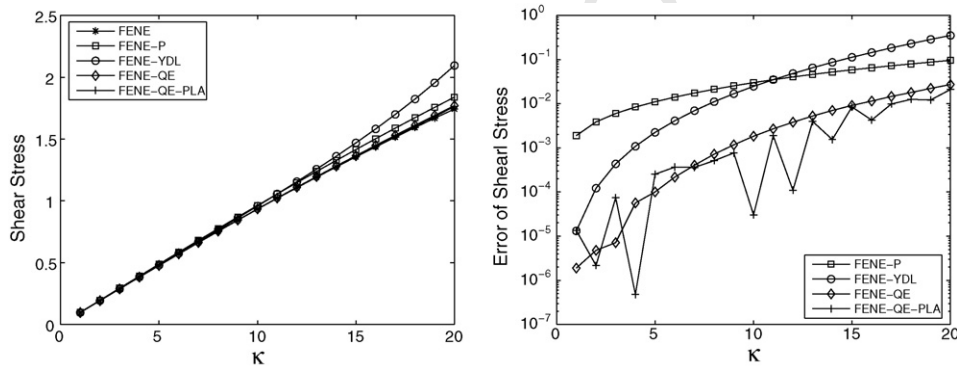


Fig. 4. Shear flow: shear stress (left) and the error plot (right) of different methods.

CDF errors do not increase quickly. When κ is equal to 20, it does as well as FENE-QE and FENE-QE-PLA. In addition, the precision of FENE-QE-PLA matches that of FENE-QE. So the PLA technique has little effect on the calculation of CDF.

Now we compare the stresses tensor obtained from the FP and other methods. When κ is not very big ($\kappa = 3-9$), FENE-YDL gives a worse approximation to CDF than FENE-P, but it approximates stress tensor more precisely (Table 1 and Figs. 3 and 4). We can observe the same phenomena with FENE-QE and FENE-P, when $\kappa = 20$. These facts support our argument that the precision of CDFs and the precision of the stress tensor sometimes varies independently. As the shear rate κ grows bigger, the errors of all closure models increase correspondingly. The results of FENE-QE and FENE-QE-PLA are better than other models;

their differences are negligible. This allows us to use FENE-QE-PLA in more complex flow fields. In Fig. 5, we compare the elastic energy $\langle U \rangle = \int U f d\mathbf{Q}$ resulting from different methods. We observe phenomena similar to previous comparisons.

We compare the CPU time of the FENE-QE that uses Newtonian iteration at each time level to obtain \mathbf{G}^{-1} and the FENE-QE-PLA that uses PLA technique. The dramatic difference of computational costs presented by Table 2 gives evidence to that the PLA technique can help reducing computational cost greatly. We should attribute the low efficiency of FENE-QE to the evaluation of $\mathbf{G}(\mathbf{R})$ and $\nabla \mathbf{G}(\mathbf{R})$ rather than the Newtonian iteration, because typically the Newtonian iteration can converge to required precision (1×10^{-8}) in no more than five steps.

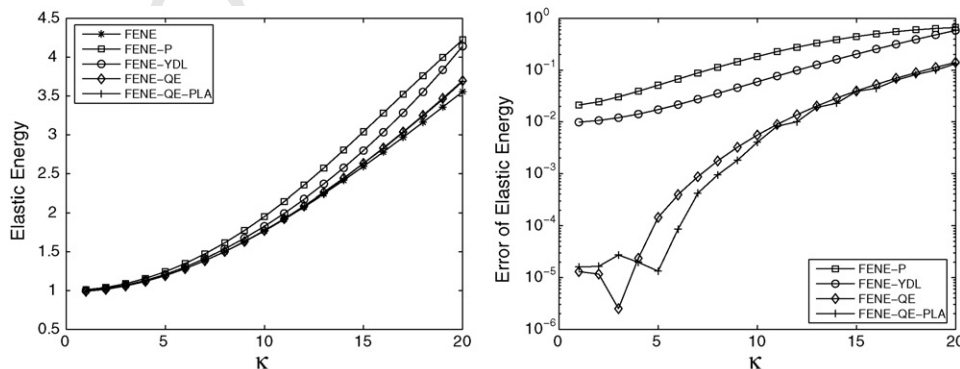


Fig. 5. Shear flow: elastic energy (left) and the error plot (right) of different methods.

Table 2
Comparison of CPU time consumed by FENE-QE and FENE-QE-PLA

Case	FENE-QE (s)	FENE-QE-PLA ($\times 10^{-2}$ s)
$\kappa = 1$	124	2.3
$\kappa = 20$	285	3.4

The experiments were run on a 3 GHz Intel Pentium IV CPU. *Note:* for PLA method, the computational cost of evaluating G^{-1} on grid points is not taken into account.

In this example, we only consider the two-dimensional configuration space. There are some three-dimensional results showing that such a simplification will not lose generality. A direct extension of two-dimensional shear flow to the three-dimensional case is to let velocity field $\mathbf{u} = (\kappa y, 0, 0)$. The BC method is used here, with physical parameters the same as those used in the two-dimensional case. The number of independent samples is $N = 10^5$. For $\kappa = 1$, the resulting stress tensor is

$$\tau_p = \begin{pmatrix} 1.0182 \times 10^0 & 9.5928 \times 10^{-2} & -1.9491 \times 10^{-4} \\ 9.5928 \times 10^{-2} & 1.0001 \times 10^0 & -1.6261 \times 10^{-5} \\ -1.9491 \times 10^{-4} & -1.6261 \times 10^{-5} & 9.9986 \times 10^{-1} \end{pmatrix} \quad (33)$$

The result here is actually time averaged to reduce variance. The normal stress difference is $\tau_p^{11} - \tau_p^{22} = 1.8104 \times 10^{-2}$ and shear stress is $\tau_p^{12} = 9.5928 \times 10^{-2}$. These are very close to the two-dimensional results: $\tau_p^{11} - \tau_p^{22} = 1.8127 \times 10^{-2}$ and $\tau_p^{12} = 9.6124 \times 10^{-2}$.

4.2. Elongation flow

Suppose $\mathbf{u} = (\kappa x, -\kappa y)$, where κ is the constant elongational rate. Divergence free condition $\nabla \cdot \mathbf{u} = 0$ is satisfied. We use the same set of physical parameters as in shear flow. FP is solved by the same finite difference method.

In Fig. 6, we give the snapshots of CDFs of FP and different closure models. When κ is small, the results of FENE-P, FENE-QE and FENE-QE-PLA are similar to those of FP, and the results of FENE-YDL are also good, except that they are not non-negative. When $\kappa > 5$, the CDFs of FP form two peaks. Only CDFs of FENE-QE and FENE-QE-PLA reflect this phenomenon. In order to show this clearly, Fig. 7 plots CDFs on the $Q_1 = 0$ line and $Q_2 = 0$ line. When κ is large, only the CDFs of FENE-QE and FENE-QE-PLA match those of FP. Moreover, FENE-P loses the double peaks when $\kappa \geq 6$. The CDFs of FENE-YDL can be negative in some regions, so that the shape

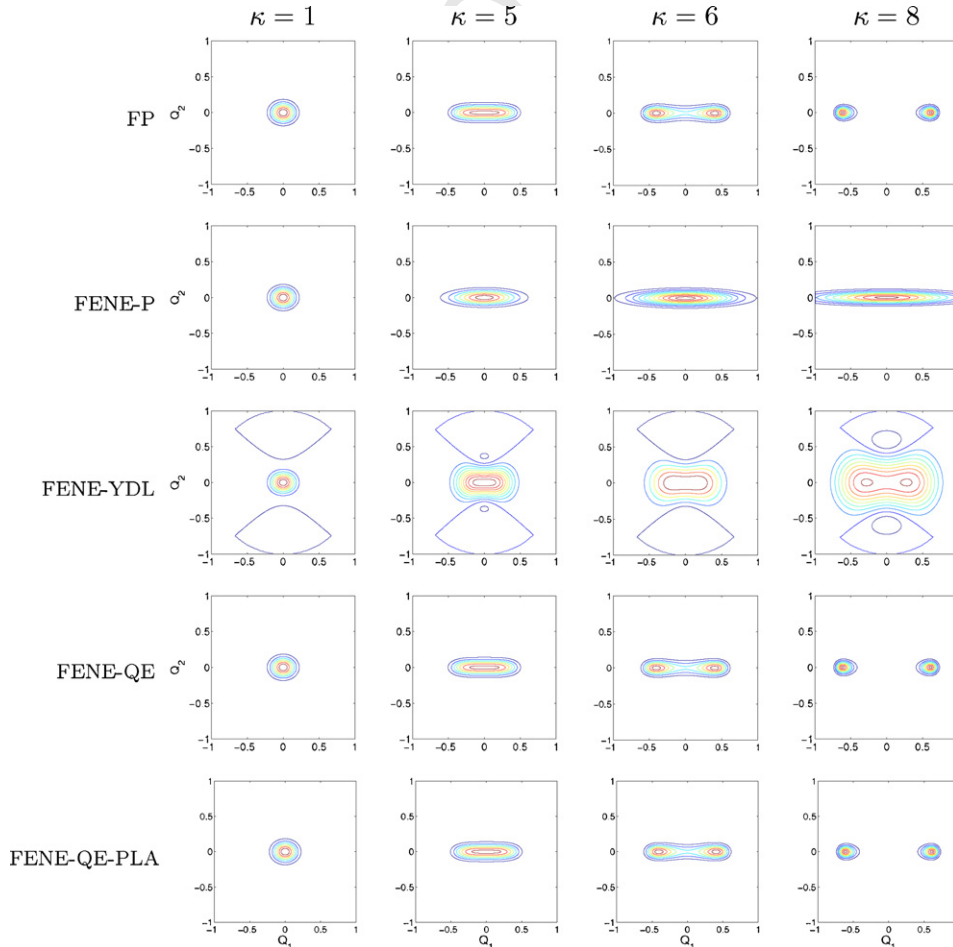


Fig. 6. Elongation flow: comparison of the contour plots of CDFs solved from the FP and different closure models for $\kappa = 1, 5, 6$ and 8 .

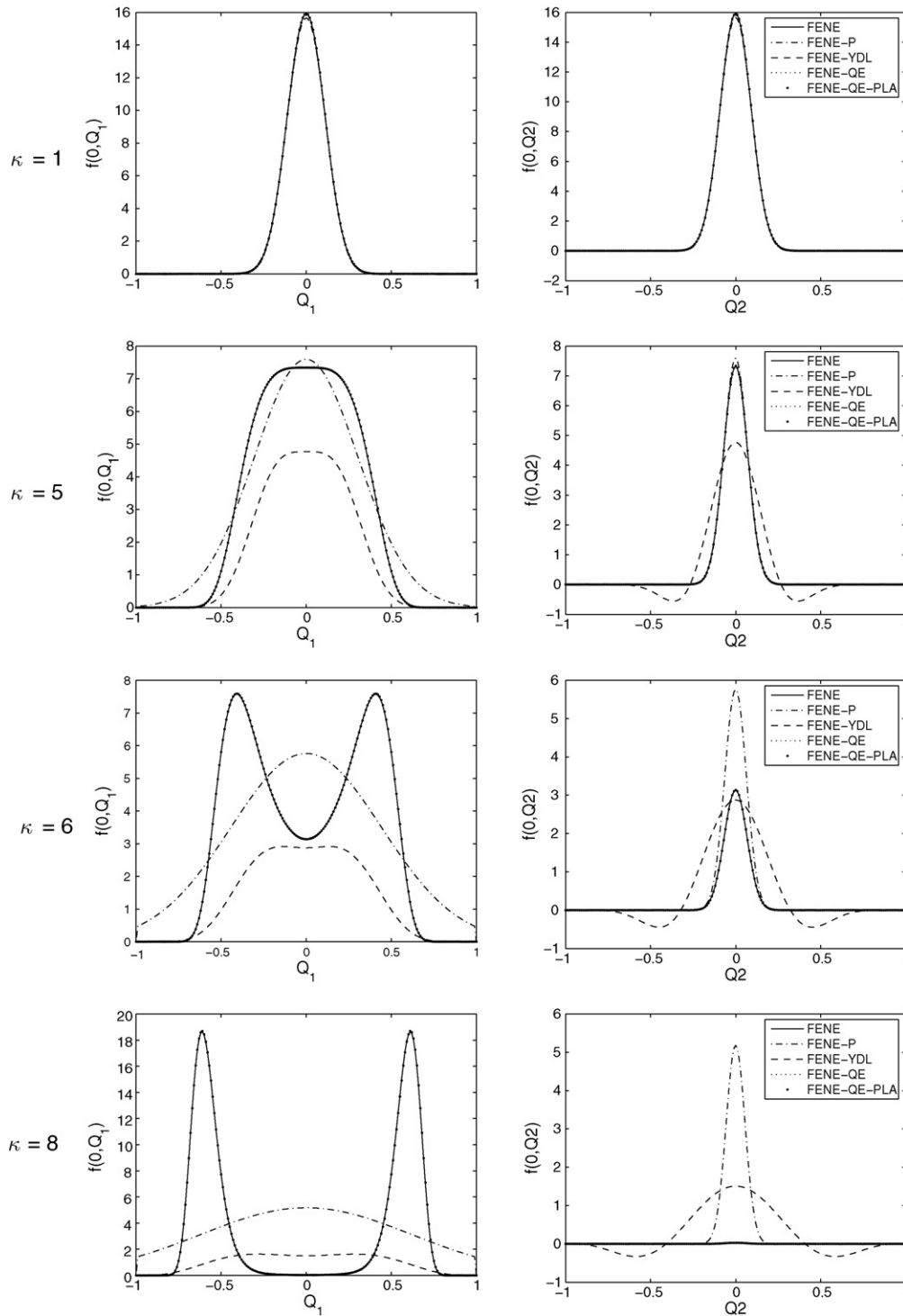


Fig. 7. Elongation flow: comparison of $f(Q_1, 0)$ (left) and $f(0, Q_2)$ (right) for $\kappa = 1, 5, 6$ and 8 (from top to bottom).

470 of CDFs differ from the CDFs of FP greatly. In fact, we can
 471 attribute the deteriorated performance of FENE-P for large κ
 472 to the fact that the CDFs of FENE-P belong to the canonical
 473 distribution subspaces every element of which has one peak. By
 474 contrast, it is not surprising that CDFs of FENE-QE are similar
 475 to the correct ones, because there exist double peak elements in its
 476 distribution function space. The L^1 errors of CDFs of different

models are given in Table 3.

We also compare the stresses and elastic energy. Because
 the shear stress is equal to zero in this case, we only give the
 normal stress difference and elastic energy in Figs. 8 and 9. We
 can see that the normal stress difference and the elastic energy
 of FENE-QE and FENE-QE-PLA are overlapped with those
 of FP in the left plots of Figs. 8 and 9. When the double peak

477
 478
 479
 480
 481
 482
 483

Table 3
Elongation flow: L^1 error of the CDFs

κ	FENE-P	FENE-YDL	FENE-QE	FENE-QE-PLA
1	1.21×10^{-2}	1.64×10^{-2}	8.35×10^{-4}	8.55×10^{-4}
2	1.75×10^{-2}	7.39×10^{-2}	8.50×10^{-4}	9.00×10^{-4}
3	3.22×10^{-2}	1.88×10^{-1}	9.26×10^{-4}	9.83×10^{-4}
4	7.55×10^{-2}	3.83×10^{-1}	1.03×10^{-3}	1.09×10^{-3}
5	1.99×10^{-1}	6.62×10^{-1}	1.23×10^{-3}	1.23×10^{-3}
6	5.25×10^{-1}	9.93×10^{-1}	1.42×10^{-3}	1.42×10^{-3}
7	1.01×10^0	1.46×10^0	1.65×10^{-3}	1.73×10^{-3}
8	1.32×10^0	1.74×10^0	2.43×10^{-3}	2.44×10^{-3}

of CDF forms ($\kappa \geq 6$), results of FENE-P and FENE-YDL deviate from FP greatly, while FENE-QE and FENE-QE-PLA still give accurate values.

5. Example: lid-driven cavity

The lid-driven cavity serves over and over again as a model problem for testing and evaluating numerical techniques in incompressible computational fluid dynamics. Here we will use it to test the numerical performance of FENE-QE-PLA and other closure approximations in a coupled system (10), (11), (26) and (27).

The method we used to discretize the incompressible Navier–Stokes equations (10) and (11) is the standard projection method [4]. Generally speaking, the solution is advanced one time step in two stages. In the first stage, the momentum

equation (10) is solved for an intermediate velocity which is not necessarily divergence free. In the second stage, that velocity is revised by the pressure gradient, which is calculated by solving a Poissonian equation with a Neumann boundary condition. The revised intermediate velocity is just the velocity on the next time level, which should be divergence free. Since solving the Poissonian equation consumes a substantial portion of the total computing time in the projection method, the efficiency of the Poissonian equation solver is crucial. Our program uses the discrete cosine transform (DCT) to develop a fast solver.

The simulation area is a two-dimensional square cavity $[0, 1] \times [0, 1]$ whose top wall moves with a velocity distribution of $u(x, y = 1, t) = 16\kappa a(t)x^2(1-x)^2$ as suggested by [6]. Here κ is a constant and to start up the flow smoothly, $a(t)$ is chosen as a time-dependent factor:

$$a(t) = \begin{cases} 0.1t & 0 \leq t < 10 \\ 1 & t \geq 10 \end{cases} \quad (34)$$

A non-penetration boundary condition is adopted on the other walls. The physical variables are discretized on a staggered grid (also known as a MAC grid). This method poses the pressure and second moment in the center of a grid cell and velocities on the surfaces of a grid cell. Compared with the collocation method that poses all physical variables on the vertices of a grid cell, this kind of discretization can avoid the loss of accuracy and oscillation in pressure equations. Because of the lack of diffusion terms in the dynamics of second moment (26), we have to discretize $\mathbf{u} \cdot \nabla \mathbf{M}$ using the upwind scheme. So the numerical

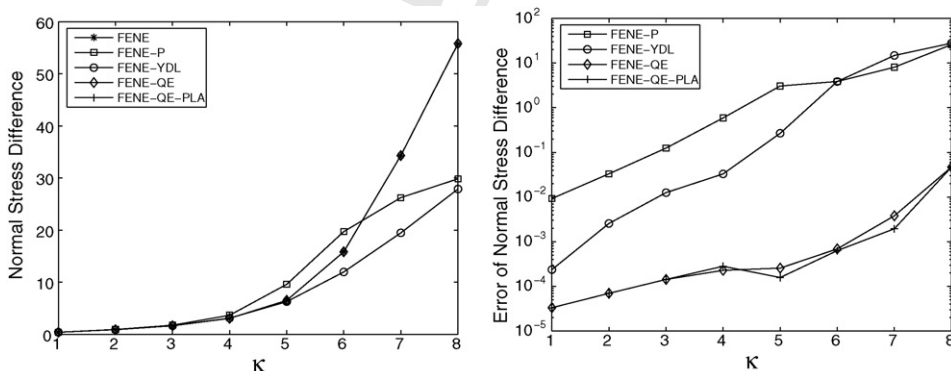


Fig. 8. Elongation flow: normal stress difference of different methods (left) and the error plot (right).

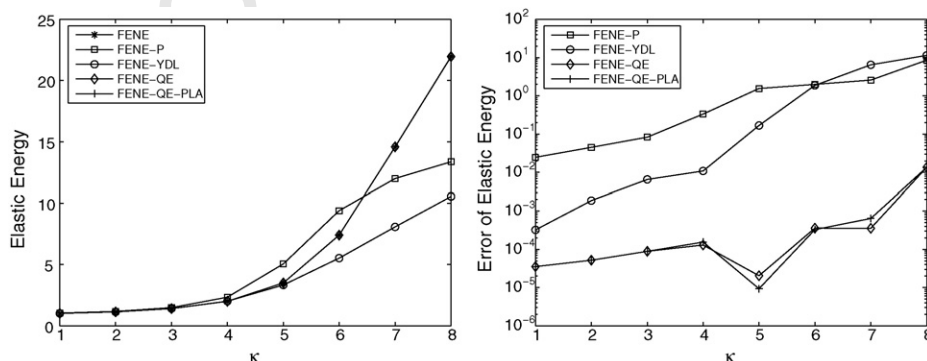


Fig. 9. Elongation flow: elastic energy of different methods (left) and the error plot (right).

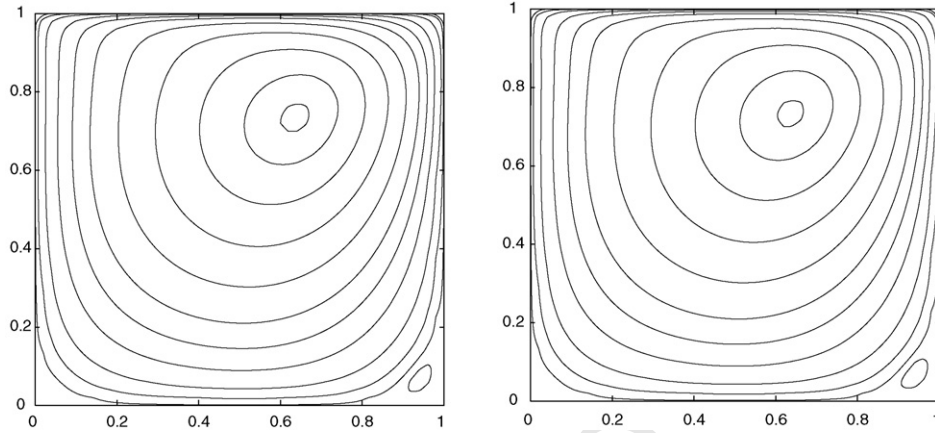


Fig. 10. Stream line of lid-driven cavity, $\kappa = 1$ at $t = 40$. BCF method (left) and FENE-QE-PLA method (right).

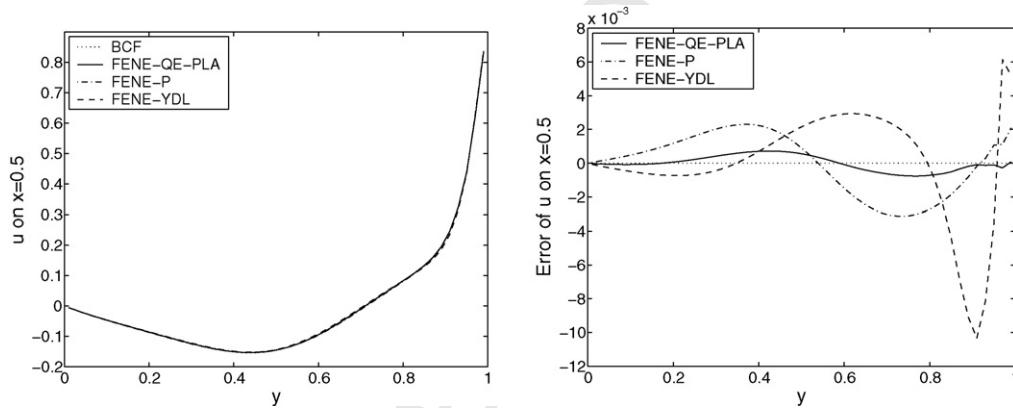


Fig. 11. Horizontal velocity distribution on line $x = 1/2$ (left) and its error plot (right), $\kappa = 1$ at $t = 40$.

flux on a vertical surface of a grid cell is

$$F_{\text{vert}} = \begin{cases} u \frac{M_l}{\Delta x} & u \geq 0 \\ u \frac{M_r}{\Delta x} & u < 0 \end{cases} \quad (35)$$

where M_l and M_r are the moments defined in the left and right cell on the surface, respectively. We choose the explicit Euler scheme to discretize the temporal term. The original FENE-QE closure approximation is too computationally expensive to

simulate a lid-driven cavity, so we are evaluating only FENE-QE-PLA.

We will consider the case $\kappa = 1$ and choose the physical parameters as $Q_0 = 1$, $n = 0.05$, $\nu = 10^{-3}$, $\zeta = 40$ and $H = 100$. The results of the BCF method serve as an “exact” solution to the problem. Since BCF is computationally expensive, we only use a uniform 50×50 grid on the physical domain. The number of independent samples is $N = 4000$. To reduce the variance, the results of BCF are time averaged. The streamline generated by the BCF method at time $t = 40$ is shown in Fig. 10

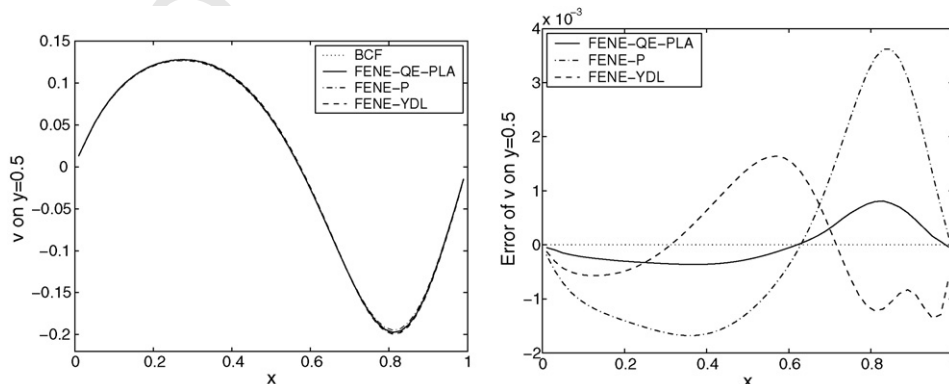


Fig. 12. Vertical velocity distribution on line $y = 1/2$ (left) and its error plot (right), $\kappa = 1$ at $t = 40$.

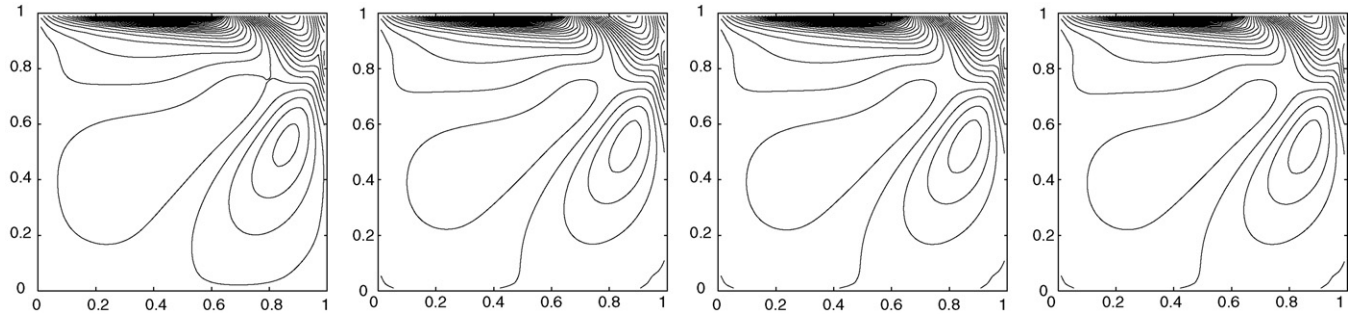


Fig. 13. Contour plot of normal stress difference. From left to right are BCF, FENE-QE-PLA, FENE-P and FENE-YDL, respectively.

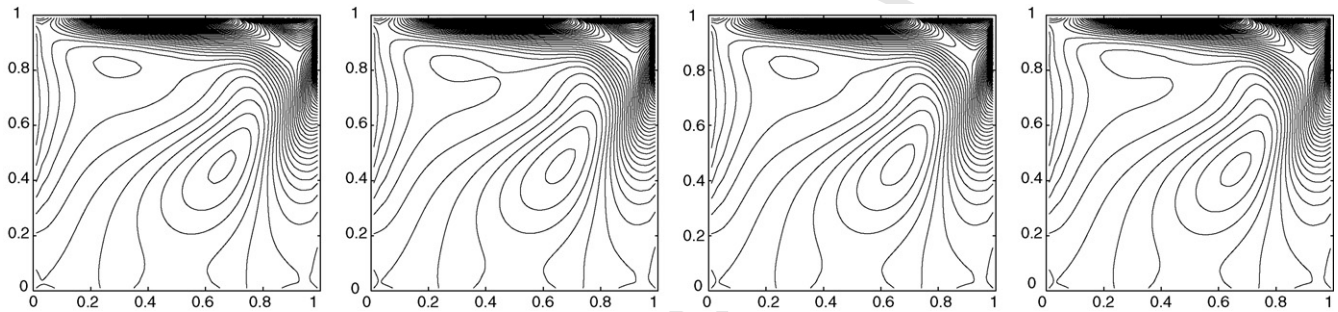


Fig. 14. Contour plot of shear stress. From left to right are BCF, FENE-QE-PLA, FENE-P and FENE-YDL, respectively.

(left). The streamline plots of the closure approximations show no significant differences from that of BCF, so we only show that of FENE-QE in Fig. 10 (right). A more detailed comparison of velocity fields is given in Figs. 11 and 12, which present the horizontal velocity distribution on $x = 0.5$ and the vertical velocity distribution on $y = 0.5$. From the velocity distribution shown in the left-hand plots in these figures, we can see that there does not exist any notable difference between the different closure methods. The error plots of the velocity distributions are shown in the right-hand plots of Figs. 11 and 12. As to FENE-QE-PLA, FENE-P and FENE-YDL, the L^2 errors of horizontal velocity distribution on $x = 0.5$ are 4.84×10^{-4} , 1.79×10^{-3} and 3.20×10^{-3} , respectively. While the errors of vertical velocity distribution on $y = 0.5$ are 3.83×10^{-4} , 1.76×10^{-3} and 9.16×10^{-4} . Therefore, we conclude that the FENE-QE-PLA is more precise than the other two closure approximations. This is the same conclusion we reached in the decoupled examples of shear flow and elongational flow. The stress tensor of these methods are presented in Figs. 13 and 14, and, again, there is no significant difference.

The CPU time consumed by FENE-QE-PLA, FENE-P and FENE-YDL are 716, 96 and 102 s, respectively. The calculation of \mathbf{G}^{-1} on grid points in the PLA algorithm is not taken into account here. While these experiments are carried out on a 3 GHz Intel Pentium IV CPU, the BCF consumed $1.7 \times 10^4 \times 10$ s on ten 3.2 GHz Intel Xeon CPUs running in parallel. It is obvious that closure models can dramatically reduce the computational cost of simulating dilute polymer solutions. The FENE-QE-PLA takes more time than FENE-P and FENE-YDL, because it has to transform \mathbf{M} into a diagonal form, to retransform $\mathbf{M} \cdot \mathbf{R}$ back to a full matrix and to execute the PLA process.

6. Conclusion

In this paper, we investigate four crucial properties for testing and evaluating moment closure approximations of the FENE dumbbell model for dilute polymer solutions. They are non-negative CDF, energy dissipation, accuracy of approximation and computational expense. The non-negativity of CDF is relatively easy to discuss because the CDF of FENE-QE, FENE-P and FENE-YDL can be written down explicitly. FENE-QE and FENE-P have non-negative CDFs, while FENE-YDL does not.

Regardless of the background flow field, we have proved that the energy dissipation behavior FENE-QE approximates that of original kinetic theory. This result can be easily extended to coupled systems that take the background flow field into account. Although the energy dissipation property is not preserved by FENE-YDL, it remains a good approximation when the state is close to equilibrium [28]. For FENE-P, we cannot yet prove the energy dissipation, but Hu and Lelièvre [9] prove energy dissipation by defining a different type of entropy.

We employ examples of shear flow and elongational flow as simple tests for decoupled systems. FENE-QE provides good precision to both CDF and stress tensor compared with the other closure models. When the shear/elongational rate grows big, the deviation of FENE-QE also increases, so it is not a good approximation in the extreme cases. The classical test problem in incompressible computational fluid dynamics, a lid-driven cavity, is used in this paper as a test for coupled systems. Careful comparisons of the resulting fluid field show that FENE-QE-PLA has the best accuracy.

One important disadvantage of the original FENE-QE is its high computational cost. The PLA technique we have introduced

can reduce this cost by four orders of magnitude. Meanwhile, numerical results of shear flow and elongational flow show that introducing the PLA technique to FENE-QE does not reduce its accuracy. The computational cost of FENE-QE-PLA is still seven to eight times over that of FENE-P and FENE-YDL. This cost can be further reduced by a detailed analysis of G^{-1} .

Generally speaking, the FENE-QE-PLA model is a high quality closure approximation method recommended for computer simulation of dilute polymer solutions. Further research will focus on the relationship between the number of moments introduced and accuracy, and on a chain-shaped model as an extension to the dumbbell model.

Q1 Uncited reference

[29].

Acknowledgements

The authors gratefully acknowledge Haijun Yu for our valuable discussions and Sharon Murrell for her help editing our English. The parallel computing was executed on a HP Linux Cluster CCSE-I (HP DL360 G4), so we would like to express the deepest gratitude to the substantial help of computer center and CCSE. Pingwen Zhang is partially supported by the special funds for Major State Research Projects 2005CB321704 and National Science Foundation of China for Distinguished Young Scholars 10225103 and 20490222.

References

- [1] R.B. Bird, C.F. Curtiss, R.C. Armstrong, O. Hassager, Dynamics of Polymeric Liquids, vol. 2: Kinetic Theory, 2nd ed., Wiley, New York, 1987.
- [2] C. Chauviere, J.N. Fang, A. Lozinski, R.G. Owens, On the numerical simulation of flows of polymer solutions using high-order methods based on the Fokker–Planck equation, *Int. J. Mod. Phys. B* 17 (2003) 9–14.
- [3] M.D. Chilcott, J.M. Rallison, Creeping flow of dilute polymer solutions past cylinders and spheres, *J. Non-Newton. Fluid Mech.* 29 (1988) 381.
- [4] A.J. Chorin, Numerical solution of the Navier–Stokes equations, *Math. Comput.* 22 (1968) 745–762.
- [5] Q. Du, C. Liu, P. Yu, FENE dumbbell models and its several linear and nonlinear closure approximations, *SIAM J. Multiscale Model. Simul.* 4 (2005) 709–731.
- [6] W. E, J. Liu, Vorticity boundary condition and related issues for finite difference schemes, *J. Comput. Phys.* 124 (1996) 368–382.
- [7] M.A. Fontelos, J. Li, On the evolution and rupture of filaments in Giesekus and FENE models, *J. Non-Newton. Fluid Mech.* 118 (2004) 1–16.
- [8] M. Herrchen, H.C. Öttinger, A detailed comparison of various FENE dumbbell models, *J. Non-Newton. Fluid Mech.* 68 (1997) 17–42.
- [9] D. Hu, T. Lelièvre, New entropy estimates for the Oldroyd-B model, and related models, <http://arxiv.org/abs/math.NA/0703198>.
- [10] M.A. Hulsen, A.P.G. van Heel, B.H.A.A. van den Brule, Simulation of viscoelastic flows using Brownian configuration fields, *J. Non-Newton. Fluid Mech.* 70 (1997) 79–101.
- [11] P. Ilg, I.V. Karlin, H.C. Öttinger, Canonical distribution functions in polymer dynamics. I. Dilute solutions of flexible polymers, *Physica A* 315 (2002) 367–385.
- [12] R. Keunings, On the Peterlin approximation for finitely extensible dumbbells, *J. Non-Newton. Fluid Mech.* 68 (1997) 85–100.
- [13] M. Laso, H.C. Öttinger, Calculation of viscoelastic flow using molecular models: the CONNFESSIT approach, *J. Non-Newton. Fluid Mech.* 47 (1993) 1–20.
- [14] A.G. Lee, E.S.G. Shaqfeh, B. Khomami, A study of viscoelastic free surface flows by the finite element method: Hele–Shaw and slot coating flows, *J. Non-Newton. Fluid Mech.* 108 (2002) 327–362.
- [15] G. Lielens, P. Halin, I. Jaumain, R. Keunings, V. Legat, New closure approximations for the kinetic theory of finitely extensible dumbbells, *J. Non-Newton. Fluid Mech.* 76 (1998) 249–279.
- [16] G. Lielens, R. Keunings, V. Legat, The FENE-L and FENE-LS closure approximations to the kinetic theory of finitely extensible dumbbells, *J. Non-Newton. Fluid Mech.* 87 (1999) 179–196.
- [17] A. Lozinski, C. Chauviere, A fast solver for Fokker–Planck equation applied to viscoelastic flows calculations: 2D FENE model, *J. Comput. Phys.* 189 (2003) 607–625.
- [18] A. Lozinski, R.G. Owens, J. Fang, A Fokker–Planck-based numerical method for modelling non-homogeneous flows of dilute polymeric solutions, *J. Non-Newton. Fluid Mech.* 122 (2004) 273–286.
- [19] H.C. Öttinger, B.H.A.A. van den Brule, M.A. Hulsen, Brownian configuration fields and variance reduced CONNFESSIT, *J. Non-Newton. Fluid Mech.* 70 (1997) 255–261.
- [20] H.C. Öttinger, A model of dilute polymer solutions with hydrodynamic interaction and finite extensibility. I. Basic equations and series expansions, *J. Non-Newton. Fluid Mech.* 26 (1987) 207–246.
- [21] J. Rimmelpas, P. Singh, L.G. Leal, Computational studies of nonlinear elastic dumbbell models of Boger fluids in a cross-slot flow, *J. Non-Newton. Fluid Mech.* 88 (1999) 31–61.
- [22] J. Rimmelpas, L.G. Leal, N.V. Orr, T. Sridhar, Viscous and elastic stresses in extensional rheometry, *J. Non-Newton. Fluid Mech.* 76 (1998) 111–135.
- [23] G.N. Rocha, R.J. Poole, P.J. Oliveira, Bifurcation phenomena in viscoelastic flows through a symmetric 1:4 expansion, *J. Non-Newton. Fluid Mech.* 141 (2007) 1–17.
- [24] R. Sizaire, G. Lielens, I. Jaumain, R. Keunings, V. Legat, On the hysteretic behaviour of dilute polymer solutions in relaxation following extensional flow, *J. Non-Newton. Fluid Mech.* 82 (1999) 233–253.
- [25] R. Sizaire, V. Legat, Finite element simulation of a filament stretching extensional rheometer, *J. Non-Newton. Fluid Mech.* 71 (1997) 89–107.
- [26] A.J. Szeri, A deformation tensor model for nonlinear rheology of FENE polymer solutions, *J. Non-Newton. Fluid Mech.* 92 (2000) 1–25.
- [27] H. Yu, G. Ji, P. Zhang, A kinetic theory of liquid crystal polymers and its thermodynamic closure approximation, *Phys. Rev. E*, in preparation.
- [28] P. Yu, Q. Du, C. Liu, From micro to macro dynamics via a new closure approximation to the FENE model of polymeric fluids, *SIAM J. Multiscale Model. Simul.* 3 (2005) 895–917.
- [29] Q. Zhou, R. Akhavan, Cost-effective multi-mode FENE bead-spring models for dilute polymer solutions, *J. Non-Newton. Fluid Mech.* 116 (2004) 269–300.